Applied Physics Letters

Investigation of trapping levels in p-type Zn_3P_2 nanowires using transport and optical properties

Cite as: Appl. Phys. Lett. **112**, 193103 (2018); https://doi.org/10.1063/1.5026548
Submitted: 21 February 2018 . Accepted: 25 April 2018 . Published Online: 09 May 2018

G. A. Lombardi, F. M. de Oliveira, M. D. Teodoro, and A. J. Chiquito

View Online

Export Citation

CrossMark

ARTICLES YOU MAY BE INTERESTED IN

High p-type doping, mobility, and photocarrier lifetime in arsenic-doped CdTe single crystals
Applied Physics Letters **112**, 192101 (2018); https://doi.org/10.1063/1.5029450

Altering thermal transport by strained-layer epitaxy
Applied Physics Letters **112**, 194101 (2018); https://doi.org/10.1063/1.5022097

Significant mobility improvement of amorphous In-Ga-Zn-O thin-film transistors annealed in a low temperature wet ambient environment
Applied Physics Letters **112**, 193501 (2018); https://doi.org/10.1063/1.5026515

Challenge us.
What are your needs for periodic signal detection?

Zurich Instruments

Watch

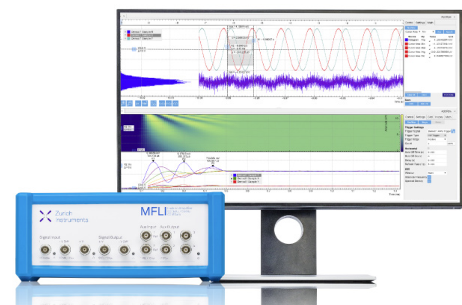

© 2018 Author(s).

AIP Publishing

Investigation of trapping levels in p-type Zn_3P_2 nanowires using transport and optical properties

G. A. Lombardi,[1] F. M. de Oliveira,[2] M. D. Teodoro,[2] and A. J. Chiquito[1,a)]
[1]*NanO LaB—Departamento de Física, Universidade Federal de São Carlos, CEP 13565-905, CP 676 São Carlos, São Paulo, Brazil*
[2]*Grupo de Nanoestruturas Semicondutoras—Departamento de Física, Universidade Federal de São Carlos, CEP 13565-905, CP 676 São Carlos, São Paulo, Brazil*

(Received 21 February 2018; accepted 25 April 2018; published online 9 May 2018)

Here, we report the synthesis and structural characterization of high-quality Zn_3P_2 nanowires via chemical vapour deposition. Structural and morphological characterization studies revealed a reliable growth process of long, uniform, and single-crystalline nanowires. From temperature dependent transport and photoluminescence measurements, we have observed the contribution of different acceptor levels (15, 50, 70, 90, and 197 meV) to the conduction mechanisms. These levels were associated with zinc vacancies and phosphorous interstitial atoms which assigned a p-type character to this semiconductor. From time resolved photoluminescence experiments, a 91 ps lifetime decay was found. Such a fast lifetime decay is in agreement with the exciton transition along the bulk emission from high quality crystalline nanowires. *Published by AIP Publishing.*
https://doi.org/10.1063/1.5026548

Nanotechnology has played a fundamental role in the advance of several research areas for the last few decades. New photovoltaic devices based on nanostructures are candidates for making a revolution on the performance of currently used devices. Nanowire based solar cells present a high surface-to-volume ratio and a small effective channel, which increase their photosensitivity and decrease their carrier transit time in comparison with bulk forms.[1–6] Other advantages of the nanowire geometry in solar power conversion include light trapping, bandgap tuning, and reduced reflection. Nanowire based photovoltaic devices also have the potential to reduce the costs and material consumption compared to the present planar technologies.[7–10] As a matter of fact, the nanowire geometry is not expected to increase the energy efficiency conversion rates but rather reduces the amount of material used for device fabrication.

A promising material for photovoltaic applications which also meets the above ideas is the II-V compound Zinc Phosphide (Zn_3P_2). Due to its elemental component abundance, Zn_3P_2 is a good candidate for low cost large-scale device production. Zn_3P_2 crystallizes in a tetragonal structure ($c/a \simeq 1.414$) but presents a pseudo-cubic lattice,[11] and it is a naturally p-type direct bandgap semiconductor with a sharp optical absorption in the near-infrared region ($\sim$1.5 eV). Additional advantages include a large absorption coefficient ($>10^4\,cm^{-1}$) and a long minority diffusion length (13 μm), which allow high current collection efficiency.[12–17] The properties of Zn_3P_2 were mainly studied in the polycrystalline phase of the material: in a very comprehensive work, Misiewicz has studied chemical vapor synthesized samples and found a large amount of acceptor carrier traps driving the optical and electrical characteristics of the material;[11] Bhushan and Catalano have shown that polycrystalline Zn_3P_2 exhibits an energy conversion efficiency of $\sim$6%.[18] There are also some different methods to synthesize high quality Zn_3P_2 nanowires in the literature.[19–22] Recently, Liu *et al.* have built a field effect transistor using Zn_3P_2 nanowires showing a good electrical performance.[22] Im *et al.* have used an alloy of Zn_3P_2 and Zn_3As_2 nanowires to be able to tune their electrical and optical properties. They found a photoconversion efficiency dependent on the growth orientation for both single and twinned nanowires.[21]

Here, we report the synthesis and structural characterization of high-quality Zn_3P_2 nanowires via the chemical vapour deposition (CVD) method using a 3-zone furnace, which allowed us to independently control the temperatures of each precursor material and the synthesis region. This method was effective in synthesizing a large amount of high quality Zn_3P_2 nanowires in a short period of time. Structural and morphological characterization studies revealed a reliable growth process of long, uniform, and single crystalline nanowires. Several devices were built with these nanowires, and the mechanisms underlying the electrical properties have been studied. From temperature dependent measurements, we have investigated the contribution of different trapping levels in Zn_3P_2 to the conduction mechanisms, which were also observed in optical emission at cryogenic temperatures. These levels were then associated with zinc vacancies and phosphorous interstitial atoms which assigned a p-type character to this semiconductor.

Zn_3P_2 nanowires were synthesized by the vapour-liquid-solid (VLS) method[23] using gold nanoparticles as catalysts. The nanoparticles act as preferential sites for the absorption of the precursor material vapour and were prepared by thermal annealing of a 20 Å Au layer deposited over Si substrates. Zinc pieces and indium phosphide (InP) powder (mass ratio 1:1) were inserted along with the Si substrates in a quartz tube and then placed inside a 3-zone tube furnace (Thermo Scientific Lindberg/Blue-M). Before heating, the furnace was evacuated to 10^{-2} Torr and purged by 10% H_2 in He flux to avoid the presence of oxygen in the synthesis chamber. Next, each zone furnace was continuously and independently heated until the local temperatures for the InP, Zn, and nanoparticle

[a)]Electronic mail: chiquito@df.ufscar.br

covered substrates were about 870, 750, and 500 °C, respectively. Zn and P vapours were carried downstream by a 150 sccm H_2/He flux. Hydrogen acting as forming gas was used to avoid superficial localized charges in the nanowires. The synthesis occurred at atmospheric pressure for 1 h. The reaction responsible for the formation of Zn_3P_2 via the VLS method is described by the following chemical reactions:[24]

$$Zn(s) \xrightarrow{heat} Zn(v), \tag{1}$$

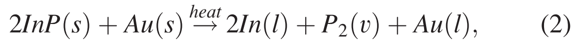

$$2InP(s) + Au(s) \xrightarrow{heat} 2In(l) + P_2(v) + Au(l), \tag{2}$$

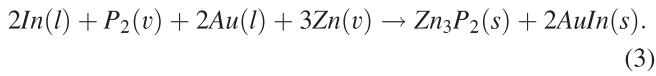

$$2In(l) + P_2(v) + 2Au(l) + 3Zn(v) \rightarrow Zn_3P_2(s) + 2AuIn(s). \tag{3}$$

After the synthesis, the substrates were covered with an ~1 mm thick brown cotton-like layer of Zn_3P_2 nanowires. X-ray diffraction (XRD, Shimadzu, XRD 6100, 40 kV, 30 mA, Cu-K monochromatic radiation) and field emission scanning electron microscopy (FEG-SEM Zeiss Supra 35) techniques were used to verify the crystallographic and morphologic features of the as-grown nanowires. Energy-dispersive X-ray spectroscopy (EDS) was used to analyse the nanowire chemical composition. TEM and HRTEM images were obtained using a FEI TECNAI F20 microscope operating at 200 kV.

Zn_3P_2 nanowires were removed from the substrate by ultrasonic agitation in ethanol solution and then dispersed on a Si/SiO_2 (oxide thickness ~500 nm) substrate. A single nanowire device was made using direct writing lithography techniques (Durham Magneto-Optics). For electrical contacts, Silver pads (100 nm thick) were deposited on substrates under high-vacuum conditions.

Electrical characterization studies were conducted in a closed cycle helium cryostat (Janis Research, CCS 400H) at pressures below 10^{-6} mbar monitored by an electrometer (Keithley Instruments, 6517B). Before temperature dependent measurements, current-voltage curves were raised in order to characterize the electrical contacts and the nanowire. Photoluminescence measurements at 3.8 K were performed using a confocal microscope (Attocube—CFMI), inserted inside a helium closed cycle cryostat (Attocube—Attodry1000). The nanowires were excited by a pulsed (80 MHz) 730 nm solid state laser (PicoQuant LDH series) and focused by an aspheric lens on a 1 μm spot with a power of 50 μW. The luminescence emitted by the sample in a backscattering configuration was collimated by the same lens and projected into a 50 μm multimode fiber connected with a 75 cm spectrometer (Andor—Shamrock), dispersed by a 150 l/mm grating, and detected using a Silicon Charged Coupled Device detector (Andor—IDUS series) for photoluminescence. Time resolved photoluminescence investigations were performed by means of a standard time correlated single photon counting technique (PicoQuant/Picoharp 300) using a dedicate Hybrid Detector (PicoQuant—PMA series).

FEG-SEM images in Fig. 1(a) show nanowires with a smooth surface, a constant diameter along the growth axis, and no lateral ramifications. The average width of the nanowires is about 230–250 nm, and they are tens of microns in length. The inset in Fig. 1(a) shows a single nanowire with a catalytic nanoparticle in its tip, which confirms the VLS growth mechanism. XRD data depicted in Fig. 1(b) are compatible with the pattern in the JCPDS #53–591 card, suggesting the as-grown nanowires with an excellent crystalline quality. The samples were indexed as a tetragonal structure with lattice constants of a = 8.121 Å and c = 11.398 Å belonging to the $P4_2/nmc$ space group. EDS data in Fig. 1(c) show the nanowire constituents, Zn and P, with an atomic ratio of ~3:2. Similar analysis in the nanoparticle shows the presence of Zn and P also with an atomic ratio of ~3:2, which is the required nanoparticle saturation to the nanowire growth. However, this saturation should be present only during the growth process. Finding the saturated nanoparticle after the synthesis may indicate that the nanowire growth was early interrupted or the excess of precursor materials was present. The Au-In alloy shown in Eq. (3) is also observed. The O signal is due to the unavoidable presence of oxygen in the analysis chamber. TEM measurements also confirmed the sample's high crystalline quality. Figure 1(d) displays a HRTEM image of an individual Zn_3P_2 nanowire. From the SAED (Selected Area Electron Diffraction) pattern, the lattice spacing was found to be 0.28 nm corresponding to the (004) plane family. The (301) plane family was also identified giving a lattice spacing of 0.26 nm and forming an angle of 71° with the nanowire's growth direction [004].

Usually, the resistance in semiconductors is described by an Arrhenius temperature dependence (thermally activated) as shown by

$$\rho(T) = \rho_0 \exp\left(\frac{\Delta E}{2k_B T}\right), \tag{4}$$

where ρ_0 is a weakly temperature-dependent factor, ΔE is an activation energy (usually the energy gap or the shallow level energy inside the gap), and k_B is the Boltzmann constant. The temperature-dependent resistance measurements are depicted in Fig. 2(a). The fitting of Eq. (4) to the experimental data reproduces well the high temperature range of the resistance dependence giving out an activation energy of 197 ± 10 meV [Fig. 2(b)]. This value agrees with the energy levels expected for zinc vacancy levels in the bulk Zn_3P_2 band structure. These vacancy levels were suggested as one of the possible origins of different acceptor levels (0.19 eV and 0.29 eV) in Zn_3P_2.[25,26] However, in the low temperature region, T < 200 K [see Fig. 2(b)], the resistance seems to be influenced by a different mechanism.

The presence of some degree of disorder which unintentionally appears in the nanowire structures drastically affects the transport of current through the nanostructure. Usually, a localized behaviour of carrier's transport and a transition from a simple excitation semiconducting mechanism to a more complex one are observed when disorder effects take place (such as the variable range hopping mechanism, VRH[27]). In systems such as those studied here, the disorder is induced by the random potential distribution of defect states, leading to the localization of carriers.[28,29]

The VRH mechanism arises when there is a sufficient amount of disorder states causing the random component of the crystalline potential to be large enough to localize the electron's wave functions near the band edges. The resistance in this case can be written as

$$\rho(T) = \rho_0 \exp\left[\left(\frac{T_0}{T}\right)^m\right], \tag{5}$$

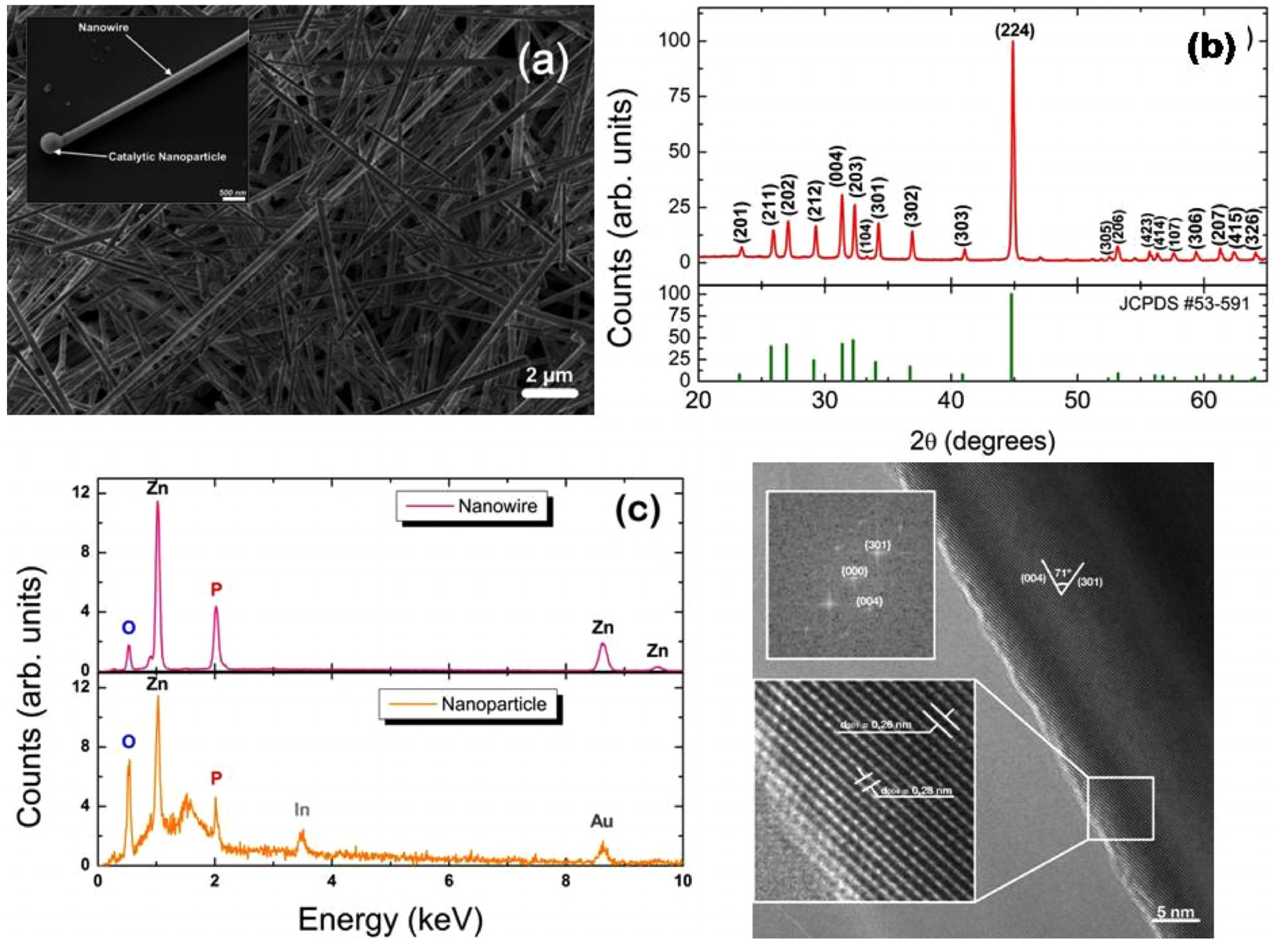

FIG. 1. FEG-SEM image of as-grown samples (a) showing a uniform distribution of nanowires. The average width is about 230–250 nm, and they are tens of microns in length; (b) XRD data compatible with the pattern in the JCPDS #53-591 card, suggesting the as-grown nanowires with an excellent crystalline quality. The samples were indexed as a tetragonal structure; (c) EDS data show that the composition of nanowires follows the atomic ratio of ∼3:2 (Zn and P). Similar analysis in the nanoparticle shows the presence of Zn and P also with an atomic ratio of ∼3:2, which is the required nanoparticle saturation to the nanowire growth; (b) HRTEM image of a single nanowire, showing the Zn_3P_2 crystalline structure and the corresponding typical single-crystalline SAED pattern (inset).

where $T_0 = 5.7\alpha^3/k_B g(E_F)$. Here, $g(E_F)$ is the density of states at the Fermi level, α^{-1} is the localization length, and $m = 1/1 + d$ where d specifies the dimensionality of the system (1, 2, or 3 for one, two, or three-dimensional structures, respectively). The VRH mechanism normally occurs in the temperature region wherein the energy is insufficient to excite the charge carriers across the Coulomb gap between two sites. Hence, conduction takes place by hopping of the small region (k_BT) in the vicinity of the Fermi level where the density of states remains almost a constant. This condition is fulfilled when the temperature is sufficiently small or when the energy states are uniformly distributed around the Fermi level.[27,30]

Fitting of Eq. (5) to the resistance data is seen in Fig. 2(c). The theoretical curve ($m = 1/4$) perfectly fits the experimental data in the whole temperature range. The mean distance that a charge can hop must be greater than the localization length (assumed as proportional to Bohr's radius), and it can be easily derived within Mott's theory framework (written for $m = 1/4$)

$$R_{hop}(T) = \alpha^{-1}\left(\frac{T_0}{T}\right)^{1/4}. \qquad (6)$$

R_{Hop} values at 100 K and 300 K were found to be 72 nm and 58 nm which are smaller than nanowire cross-sections, confirming that the nanostructures studied in this work behave as three-dimensional systems.

From the above discussion, it is found that the conduction process in Zn_3P_2 nanowire devices is governed by two different temperature-triggered mechanisms which take place at the same time. As the hopping contribution seems to be the dominant one, the thermally activated process is only able to effectively contribute at high temperatures, near room temperature as seen in Fig. 2(b). However, according to the literature, bulk Zn_3P_2 is known to present different activation energies in the range of 14–90 meV which were not detected in the measurements presented here.

In order to investigate the presence of different activation levels, thermally stimulated current (TSC) measurements were used. In this technique, the devices were initially cooled down to 77 K. If there is an electron trapping centre with energy above the normal dark Fermi level, then trapped electrons will be in a non-equilibrium state, and thereby, their rate of release will depend mainly on the phonon energy available in the lattice.[31–33] Thus, the rise of temperature after removing the optical stimulation will empty the traps to the conduction band,

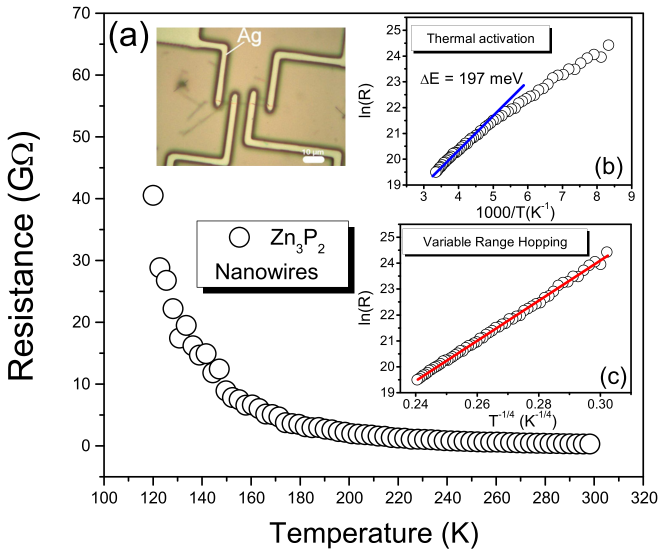

FIG. 2. (a) Temperature-dependent resistance measurements showing a semiconducting behaviour; (b) Arrhenius plot and the corresponding fitting of a thermal activated transport process. At high temperatures, the fitting provided $\Delta E = 197$ meV in accordance with zinc vacancy levels; (c) Theoretical fitting of the resistance to the VRH model for temperatures ranging from 100 to 300 K. The mean hopping distances (R_{Hop}) for 100 K and 300 K were found to be 72 nm and 58 nm which are smaller than nanowire cross-sections, confirming that the nanostructures studied in this work behave as three-dimensional systems. The inset depicts an optical microscopy image of the measured device.

which can be observed by the temporary increase in the electric current. The excess conductivity presents a maximum at a given temperature. The conductive data were then adjusted to the following equation:

$$I_{TSC}(T) = I_0 N_{C,V} \times \exp\left(-\frac{\Delta E}{k_B T} - \frac{1}{N_T \beta \tau}\int_{T_0}^{T} N_{C,V} \exp\left(-\frac{\Delta E}{k_B T}\right) dT\right), \tag{7}$$

where I_0 is related to the trap properties, $N_{C,V}$ is the number of electrons in the conduction (valence) band, τ is the carrier lifetime, N_T is the number of traps, ΔE is the activation energy necessary to release trapped carriers, T_0 is the trap filling temperature, and β is the heating rate used in the experiment.

The thermally stimulated current data for two different devices were fitted using Eq. (7) as depicted in Fig. 3: agreement between theoretical and experimental curves in the peak region is remarkable for both devices. For T > 300 K, where the thermionic emission dominates the electric current through the device, the fitting process was not used for convenience. As a result, two energy levels, 47 ± 8 meV and 15 ± 3 meV, were found accounting for trap levels inside the bandgap of Zn_3P_2.

In the literature, Zn_3P_2 is known to exhibit acceptor levels (from zinc vacancies, typically 0.19 eV and 0.29 eV) and those generated by phosphorous interstitial atoms (from 14 meV to 90 meV).[34] From resistance measurements [Arrhenius plot, 2(b)], the 197 meV level associated with zinc vacancies was identified, while from TSC experiments, other two phosphorous related levels were observed (47 and 15 meV). In order to confirm our results, low temperature photoluminescence

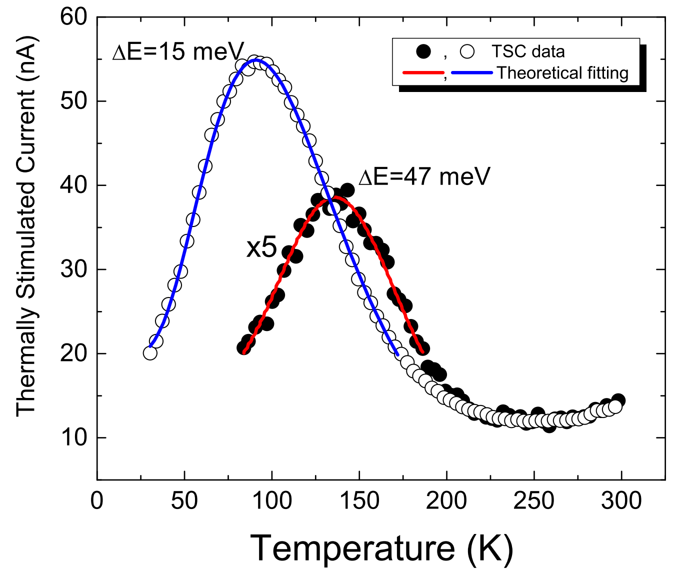

FIG. 3. Thermally stimulated current data for two devices and theoretical curve showing the carrier's emission around 150 K (47 meV) and 90 K (15 meV) both associated with acceptor energy levels.

experiments were conducted (Fig. 4). From the PL spectrum, four characteristic peaks were observed: 1.5 eV, which is in accordance with the bulk gap value; 1.45 eV, 1.43 eV, and 1.41 eV and a broadband centred at 1.30 eV. No blue-shift associated with quantum confinement size effects was observed probably due to the large width of the nanowires. The broadband centred at 1.30 eV corresponds to the zinc vacancy acceptor levels (197 meV, also observed in transport data), while peaks at 1.45 eV, 1.43 eV, and 1.41 eV correspond to phosphorous interstitial atoms (50 meV, 70 meV, and 90 meV from the valence band, respectively). The 50 meV energy level is in good agreement with that extracted out from the transport data; however, we were not able to observe energies higher than 50 meV in TSC measurements due to the thermionic emission. The 15 meV energy level was not observed in the photoluminescence spectrum probably because it is close to the band edge; in

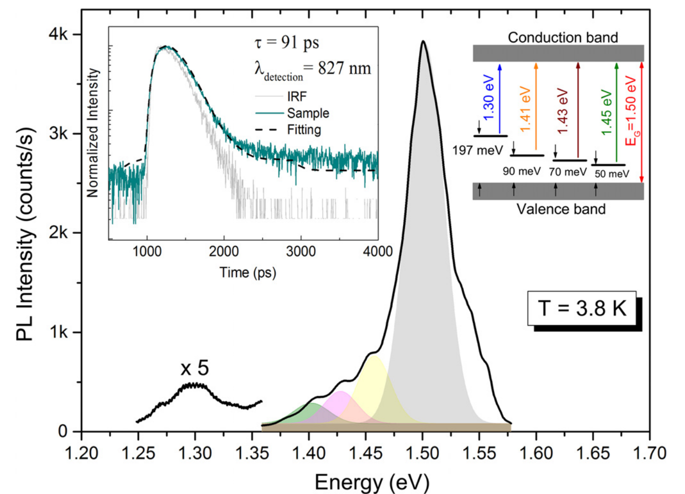

FIG. 4. Photoluminescence results taken at 3.8 K. Colour curves represent the Gaussian fittings for every peak emission. The inset presents the TRPL decay (green curve) measured at 827 nm, corresponding to the bulk gap emission. The grey color curve is the Internal Response Function (IRF) of the system. A schematic energy level diagram, based on transport and optical data, is depicted (the 15 meV level is not shown in this diagram).

order to study the dynamics of the optical transition, time resolved photoluminescence (TRPL) was obtained, centred at 827 nm, where we observed the bulk emission. As can be seen in the inset of Fig. 4, a mono-exponential decay was observed. After the deconvolution of the experimental data taking into account the Internal Response Function (IRF) of the system, we found a time decay of 91 ps. Such a fast lifetime decay is in agreement with the exciton transition along the bulk emission from high quality crystalline nanowires. The absence of a second lifetime decay as observed in the literature[35] indicates that no other recombination from the surface occurs for our samples.

In this work, we have reported the synthesis and structural, electrical, and optical characterization studies of high-quality Zn_3P_2 nanowires synthesized via the chemical vapour deposition technique. This method was effective in synthesizing a large amount of high quality Zn_3P_2 nanowires in a short period of time. Structural and morphological characterization studies revealed a reliable growth process of long, uniform, and single crystalline nanowires. Different devices were investigated, and the conduction process in Zn_3P_2 nanowires seems to be governed by two different temperature-triggered mechanisms which take place at the same time. As the hopping contribution seems to be the dominant one, the thermally activated process is only able to effectively contribute at high temperatures near to room temperature. From TSC measurements, we were able to identify some other low energy levels (15 meV and 47 meV) which were not observed in resistance measurements. The contribution of these different trapping levels in Zn_3P_2 to the conduction mechanism was also observed in optical emission at cryogenic temperatures. Using both transport and photoluminescence data, an energy diagram for the active levels inside the Zn_3P_2 gap was built.

The authors acknowledge the financial support from the Brazilian agencies Sao Paulo Research Foundation (FAPESP) under Grant Nos. 2013/17639-4, 2013/18719-1, 2014/19142-2, and 2016/14381-4; and the National Council for Scientific and Technological Development (CNPq) under Grant No. 305615/2014-9.

[1]Y. Cui, J. Wang, S. R. Plissard, A. Cavalli, T. T. T. Vu, R. P. J. van Veldhoven, L. Gao, M. Trainor, M. A. Verheijen, J. E. M. Haverkort, and E. P. A. M. Bakkers, Nano Lett. **13**, 4113 (2013).
[2]M. D. Kelzenberg, S. W. Boettcher, J. A. Petykiewicz, D. B. Turner-Evans, M. C. Putnam, E. L. Warren, J. M. Spurgeon, R. M. Briggs, N. S. Lewis, and H. A. Atwater, Nat. Mater. **9**, 239 (2010).
[3]K. L. Chopra, P. D. Paulson, and V. Dutta, Prog. Photovoltaics: Res. Appl. **12**, 69 (2004).
[4]J. S. Jie, W. J. Zhang, Y. Jiang, X. M. Meng, Y. Q. Li, and S. T. Lee, Nano Lett. **6**, 1887 (2006).
[5]Z. Fan, J. C. Ho, Z. A. Jacobson, H. Razavi, and A. Javey, Proc. Natl. Acad. Sci. U. S. A. **105**, 11066 (2008).
[6]S. L. Diedenhofen, O. T. A. Janssen, G. Grzela, E. P. A. M. Bakkers, and J. G. Rivas, ACS Nano **5**, 2316 (2011).
[7]E. C. Garnett, M. L. Brongersma, Y. Cui, and M. D. McGehee, Annu. Rev. Mater. Res. **41**, 269 (2011).
[8]W. U. Huynh, J. J. Dittmer, and A. P. Alivisatos, Science **295**, 2425 (2002).
[9]B. O'Regan and M. Grätzel, Nature **353**, 737 (1991).
[10]A. Polman and H. A. Atwater, Nat. Mater. **11**, 174 (2012).
[11]J. Misiewicz, J. Phys.: Condens. Matter **2**, 2053 (1990).
[12]S. Sudhakar, V. Ganesh, I. Sulania, P. K. Kulriya, and K. Baskar, J. Phys. D: Appl. Phys. **40**, 5071 (2007).
[13]A. Hupfer, D. Hirsch, and S. Schulze, Phys. Status Solidi B **152**, 505 (1989).
[14]J. Andrzejewski and J. Misiewicz, Phys. Status Solidi B **227**, 515 (2001).
[15]E. A. Fagen, J. Appl. Phys. **50**, 6505 (1979).
[16]P. Wu, Y. Dai, Y. Ye, Y. Yin, and L. Dai, J. Mater. Chem. **21**, 2563 (2011).
[17]C. Liu, L. Dai, L. P. You, W. J. Xu, R. M. Ma, W. Q. Yang, Y. F. Zhang, and G. G. Qin, J. Mater. Chem. **18**, 3912 (2008).
[18]M. Bhushan and A. Catalano, Appl. Phys. Lett. **38**, 39 (1981).
[19]L. Brockway, M. Van Laer, Y. Kang, and S. Vaddiraju, Phys. Chem. Chem. Phys. **15**, 6260 (2013).
[20]R. S. Yang, Y. L. Chueh, J. R. Morber, R. Snyder, L. J. Chou, and Z. L. Wang, Nano Lett. **7**, 269 (2007).
[21]H. S. Im, K. Park, D. M. Jang, C. S. Jung, J. Park, S. J. Yoo, and J.-G. Kim, Nano Lett. **15**, 990 (2015).
[22]C. Liu, L. Dai, R. M. Ma, W. Q. Yang, and G. G. Qin, J. Appl. Phys. **104**, 034302 (2008).
[23]R. S. Wagner and W. C. Ellis, Appl. Phys. Lett. **4**, 89 (1964).
[24]H. Kamimura, R. C. Gouveia, C. J. Dalmaschio, E. R. Leite, and A. J. Chiquito, Semicond. Sci. Technol. **29**, 015001 (2014).
[25]N. Mirowska and J. Misiewicz, Semicond. Sci. Technol. **7**, 1332 (1992).
[26]D. M. Stepanchikov and G. P. Chuiko, Condens. Matter Phys. **12**, 239 (2009).
[27]N. F. Mott, *Metal-Insulator Transitions* (Taylor & Francis, London 1990).
[28]G. Gu, M. Burghard, G. T. Kim, G. S. Dusberg, P. W. Chiu, V. Krstic, and S. Roth, J. Appl. Phys. **90**, 5747 (2001).
[29]R. A. Simon, H. Kamimura, O. M. Berengue, E. R. Leite, and A. J. Chiquito, J. Appl. Phys. **114**, 243705 (2013).
[30]A. J. C. Lanfredi, R. R. Geraldes, O. M. Berengue, E. R. Leite, and A. J. Chiquito, J. Appl. Phys. **105**, 023708 (2009).
[31]J. D. Prades, F. Hernandez-Ramirez, R. Jimenez-Diaz, M. Manzanares, T. Andreu, A. Cirera, A. Romano-Rodriguez, and J. R. Morante, Nanotechnology **19**, 465501 (2008).
[32]J. M. Wrobel, A. Gubanski, E. Placzek-Popko, J. Rezmer, and P. Becla, J. Appl. Phys. **103**, 063720 (2008).
[33]H. C. Wright and G. A. Allen, Br. J. Appl. Phys. **17**, 1181 (1966).
[34]A. Catalano and R. B. Hall, J. Phys. Chem. Solids **41**, 635 (1980).
[35]G. M. Kimball, A. M. Muller, N. S. Lewis, and H. A. Atwater, Appl. Phys. Lett. **95**, 112103 (2009).